<illustration>Atmospheric Chemistry and Physics Open Access EGU logo</illustration>

Supplement of

Atmospheric aerosols in Rome, Italy: sources, dynamics and spatial variations during two seasons

Caroline Struckmeier et al.

Correspondence to: Caroline Struckmeier (c.struckmeier@mpic.de) and Frank Drewnick (frank.drewnick@mpic.de)

1 Quality assurance of AMS data

As detailed in the main text, all data were corrected for sampling delays (individual transport time for each instrument in the inlet system) and inspected for instrument malfunctions or contaminations from local emissions. AMS data were analysed using the standard AMS data analysis software SQUIRREL 1.55H and PIKA 1.14H as well as APES light 1.06. In these procedures all common quality assurance steps were applied. For this purpose also measurements of filtered air were made several times during each field campaign. IE calibrations were performed before the DIAPASON and after the POPE campaigns in both years and showed no general trends in IE.

In addition to these internal AMS quality assurance measures, the time series of total AMS species plus BC were compared with time series of PM_1 from EDM measurements for each measurement campaign (Figure S1). It is assumed that the sum of all AMS species and black carbon (from the MAAP) accounts for most of the PM_1 mass and thus the concentration time series should agree. Figure S1 shows that the trends in total sub-micron aerosol concentration are very similar in both PM_1 measurements (R^2: 0.69-0.85). Nevertheless, differences between the absolute values of the mass concentrations can be observed, resulting in different slopes of the linear fits in the scatter plots for total AMS plus BC concentration plotted versus PM_1 measured by EDM (Figure S2). These differences can be explained by inherent differences in the measurement methods, as discussed in detail below.
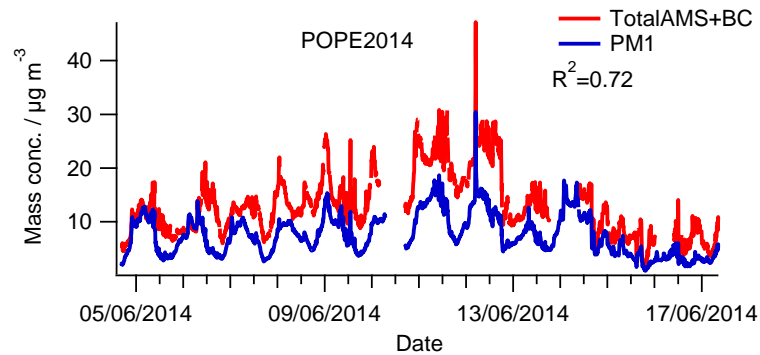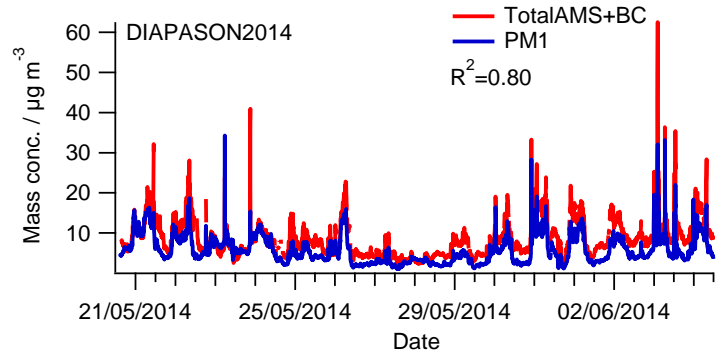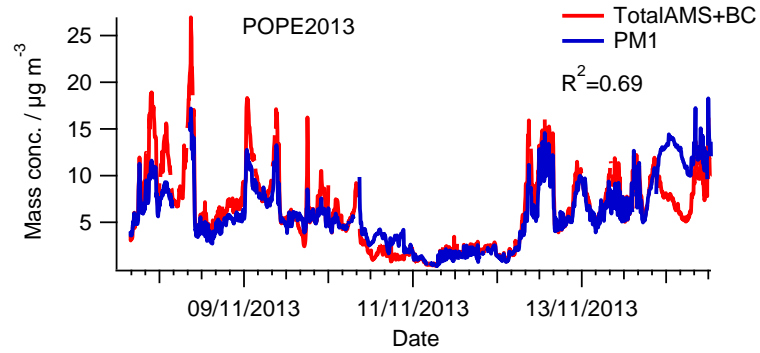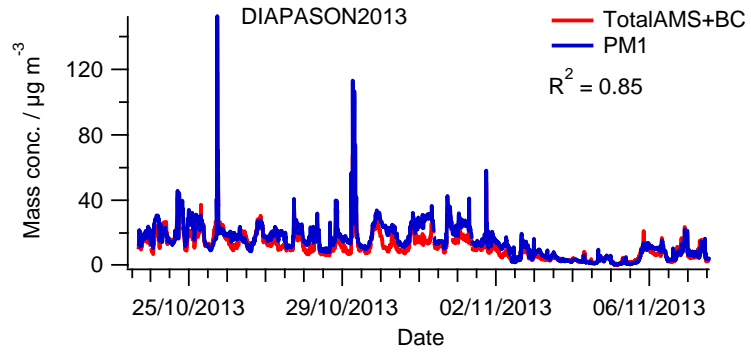
Figure S1: Time series of total AMS species plus BC concentrations (red) and PM$_1$ from EDM measurements (blue) for each measurement campaign. Pearson's R^2 for the correlation of both time series is also shown.

1
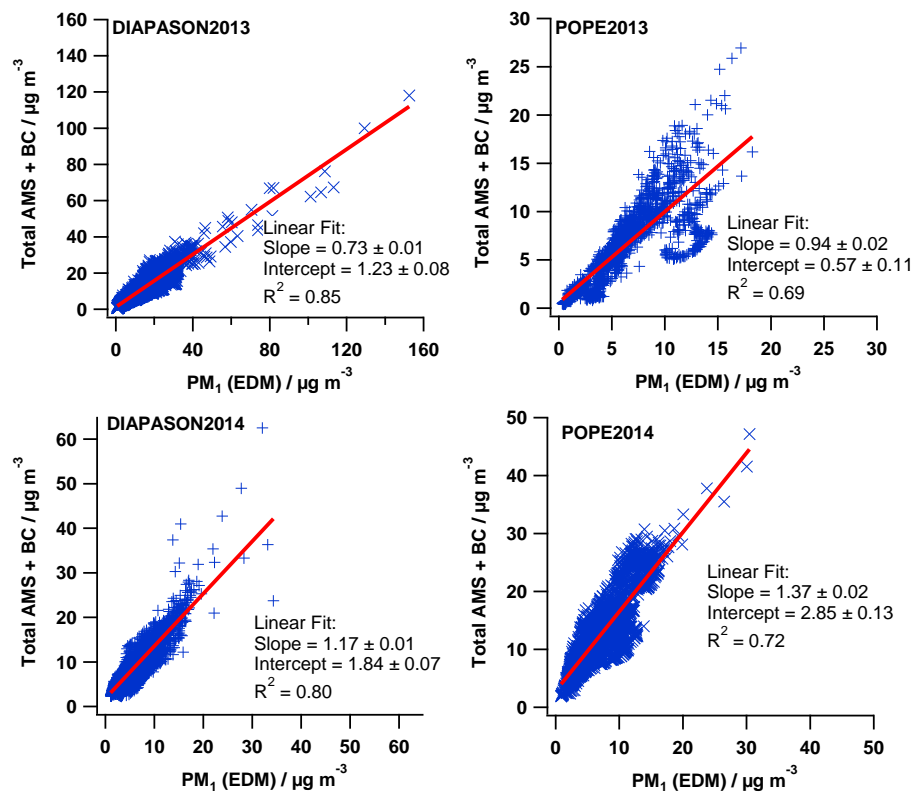
Figure S2: Scatter plot of combined total AMS species + BC concentration and PM$_1$ from EDM measurements. The slope, intercept and correlation (R^2) of the linear fit are shown.

Differences in PM$_1$ concentration determined with the combination of AMS + MAAP and with the EDM can result from various causes, inherent in the measurement methods:

- Refractory material other than BC: During the dust periods mineral dust was also found in PM$_1$ as presented in the main text. This refractory material is measured with the EDM but neither with the AMS nor the MAAP instrument. This could explain the slightly higher EDM PM$_1$ concentrations during parts of the DIAPASON 2013 campaign, especially for the period during the dust event (23.10.-01.11.13). (Figure S1).

- AMS collection efficiency: For calculation of AMS mass concentrations a collection efficiency (CE) of 0.5 was applied to all AMS data, in agreement with Canagaratna et al. (2007). Collection efficiency can increase and reach values up to 1.0 when the aerosol is liquid or has a substantial liquid layer like for high relative humidity (RH), high nitrate content, acidic aerosol or high content of liquid organic material (Middlebrook et al., 2012). Potentially liquid organic material could be e.g. HOA or SV-OOA. Variations in collection efficiency due to different aerosol composition can be accounted for by applying a time-dependent collection efficiency (Middlebrook et al., 2012). In our case, the time-resolved composition-dependent collection efficiency did always scatter closely around 0.5, and also RH was not in a range which would suggest liquid aerosol (and therefore higher collection efficiency). As shown below, the ratio of AMS+BC versus EDM PM_1 has a very distinct diurnal cycle (Figure S3, left panel). Maximum values of this ratio (i.e., AMS + BC significantly larger than EDM PM_1, which theoretically could be caused by a too small collection efficiency) are found during the afternoon when RH in the inlet line, SV-OOA concentrations (and HOA, not shown), and the nitrate fraction is low (Figure S3). The aerosol was neutralized during all measurements. Under these conditions there is no known reason for increased AMS collection efficiency and therefore this type of artefact cannot explain the differences.

- EDM measurement range: The EDM optically measures the particle size distribution and calculates PM_1 using a sophisticated but proprietary algorithm. In this calculations assumptions have to be made for the contribution of particles $d_{opt} < 250$ nm (the lower cut-off of the optical measurement). Very high concentrations of small particles (e.g. close to traffic sources) could result in PM_1 values being biased low due to shortcomings of these assumptions. However, as shown in Figure S3, small particle concentrations are not elevated during the afternoon, when the EDM shows lowest PM_1 values compared to the AMS, therefore it cannot explain the observed differences.

- Particle size – RH dependence: With decreasing relative humidity particle size can decrease as a consequence of water evaporating off the particles. Since the AMS directly measures the mass concentration of the various aerosol species it is not affected by particle water other than via the CE factor (see second bullet point). EDM on the other hand measures PM based on the particle size distribution, and therefore EDM PM_1 will depend on relative humidity in the sampling line. For this reason the instrument dries the aerosol at a relative humidity > 55 % using a Nafion drier. However, we also observe an influence on particle size at lower RH values: Figure S3 (right panel) shows a scatter plot of ratios AMS+BC / EDM PM_1 versus inlet line RH for all field campaigns. A clear increase in the ratio for low inlet line RH can be seen. Under these conditions apparently the EDM under-measures PM_1. For the 2014 (late spring) campaigns RH was especially low, resulting in the largest effect for these measurements (Figure S1).

1   In summary, we conclude that there is a reasonable agreement between the two ways of determining PM_1 with differences that can be explained by the

2   characteristics of the applied instruments and which validate the assumption of applying an AMS CE factor of 0.5.
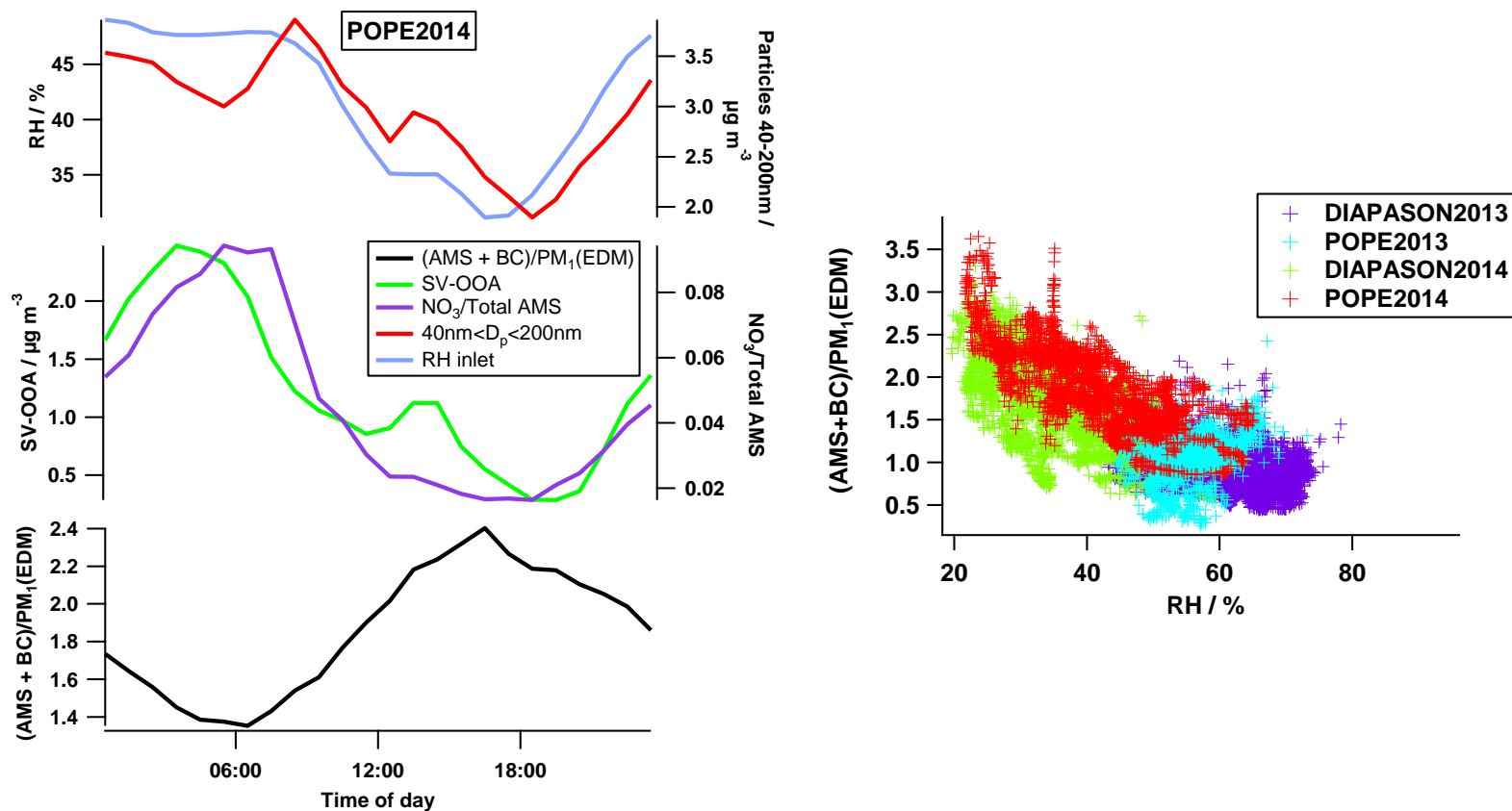
3

4 **Figure S3: Comparison of the diurnal cycle of the ratio of (AMS+BC)/PM$_1$ (EDM) with the diurnal cycles of RH in the inlet system, mass concentration (ρ=1 g cm^{-3}) of particles with**
5 **diameters 40nm<D$_p$>200nm calculated from the FMPS measurements, SV-OOA, and the contribution of NO$_3$ to total AMS mass for the POPE2014 campaign (left). Scatter plot of the**
6 **ratio of (AMS+BC)/PM$_1$ (EDM) versus relative humidity (RH) in the inlet system for each campaign (right).**

7

2 Quality assurance of AMS PMF analysis

For each measurement campaign (DIAPASON2013, POPE2013, DIAPASON2014, POPE2014) the PMF analysis of the OA fraction of high resolution AMS data was performed separately. PMF data and error input matrices were generated for organic species with m/z<131 within PIKA 1.14H. Isotopes constrained to a fractional signal of their parent ion were excluded from the analysis. Within the PMF Evaluation Tool v2.06 a minimum counting error of 1 was applied, ions with signal-to-noise ratio < 0.2 were removed from data and error matrices, and ions with signal-to-noise ratio between 0.2 and 2 were down-weighted in the analysis by increasing their estimated error by a factor of two (Ulbrich et al., 2009). Particulate CO_2^+ (m/z 44) and its associated ions at m/z 16, 17, 18 and 28 were down-weighted by a factor of $\sqrt{5}$ (Ulbrich et al., 2009, supplemental information).

In order to find the most reasonable PMF solution the number of factors was increased until no additional physically meaningful factor was obtained and only factor splitting occurred. Additionally the rotational force parameter (fPeak: -1 to 1; $\Delta = 0.2$) and the starting point (seed: 0 to 50; $\Delta = 1$) were varied. Solutions with fPeak=0 and seed=0 turned out to yield robust results for all data sets. Figure S4 presents $Q/Q_{expected}$ for PMF solutions with different numbers of factors for each measurement campaign. The selected solution is shown with an orange circle for each campaign.
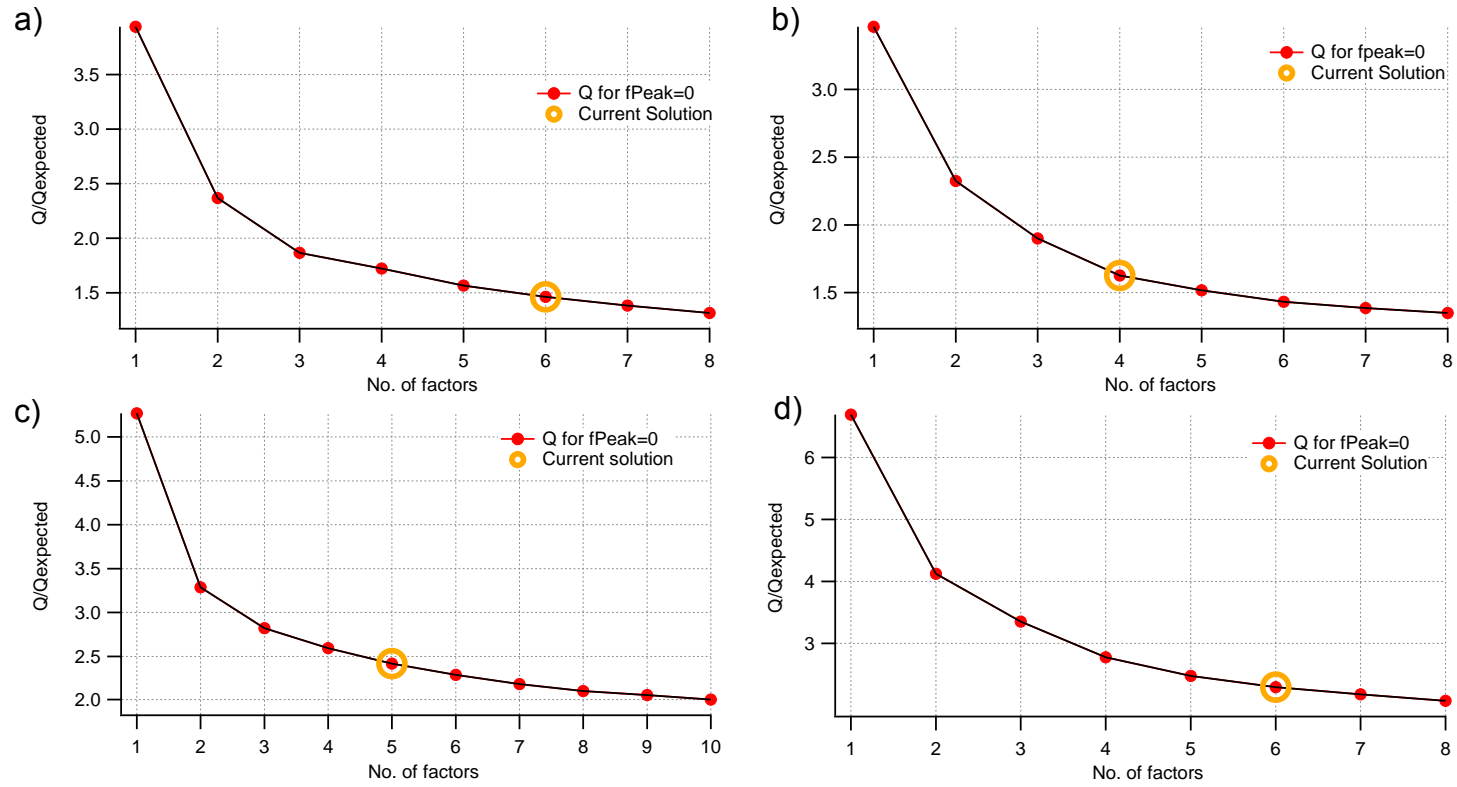
Figure S4: Q/Q$_{expected}$ for PMF solutions with different numbers of factors for a) DIAPASON2013, b) POPE2013, c) DIAPASON2014 and d) POPE2014. The chosen PMF factor solution is marked with a yellow circle.

7

1   Table S1 provides an overview of the PMF matrix input sizes and the number of factors which were chosen for each measurement campaign. The characteristics

2   (factor mass spectra, time series, elemental ratios) of each chosen PMF solution are presented in the following subsections together with information on

3   additional variables which were used to identify the respective aerosol type. The elemental ratios of the PMF factors were calculated based on the improved

4   calibration method introduced by Canagaratna et al. (2015).

5

6   **Table S1: Overview of the PMF matrix input size, the number of factors for the chosen PMF solution, and the number of identified species for each measurement campaign.**

|	DIAPASON2013	POPE2013	DIAPASON2014	POPE2014
Matrix input size (rows / columns)	20785 / 308	9670 / 317	38327 / 297	30028 / 304
Number of factors	6	4	5	6
Number of identified species	4	4	5	5
Identified species	OOA, HOA, COA, BBOA (2 OOA and 2 BBOA factors were recombined)	OOA, HOA, COA, CSOA	LV-OOA, SV-OOA, HOA, COA, BBOA	LV-OOA, SV-OOA, HOA, COA, CSOA (2 LV-OOA factors were recombined)

7

8

2.1 DIAPASON2013

For DIAPASON2013 a 6-factor solution was chosen. In this solution two factors assigned to OOA and two factors assigned to BBOA were regrouped to one OOA and one BBOA factor, respectively, using the sum of the time series and the weighted average of the mass spectra. The resulting factor mass spectra and associated mass concentration time series are shown in Figure S5 together with ancillary data. Correlations between the factor time series and those of these external tracers helped identifying the aerosol types associated with the factors (Figure S6). The mass spectra of OOA1 and OOA2 (Figure S7, left) showed correlations of $R^2 > 0.98$. The mass spectra of BBOA1 and BBOA2 are more different ($R^2 > 0.44$).The contributions of m/z 41, 44 and 55 are much more pronounced in the BBOA1 spectrum, whereas m/z 29, 60 and 73 strongly contribute to the BBOA2 spectrum. As mentioned in the manuscript, the comparison with the BBOA spectrum presented in Mohr et al. (2012) resulted in rather poor correlations. However, better correlation was obtained after recombination of BBOA1 and BBOA2 ($R^2 = 0.57$ instead of $R^2 = 0.51$ (BBOA1) and $R^2 = 0.43$ (BBOA2), respectively). Nevertheless, the main reason for combining both factors to BBOA was based on their time series (Figure S8a). As mentioned in the manuscript, in the evening of 25/10/2013 a strong biomass burning event was visually detected and attributed to agricultural waste burning in the nearby Alban Hills. Only a factor including this event was considered to be attributed to biomass burning emissions. The time series of BBOA1 and BBOA2 both show a distinct signal during this biomass burning event and also the pattern during the remaining time is similar ($R^2 > 0.61$). The diurnal cycles of BBOA1 and BBOA2 show increased concentrations during similar time periods (Figure S8b). BBOA1 is slightly shifted to earlier times compared to BBOA2. BBOA1, BBOA2 and BBOA1+2 show all reasonable correlations with the biomass burning tracer $C_3H_5O_2^+$ (Figure S8c). Careful inspection of the properties of BBOA1 and BBOA2 did not provide plausible reasons for interpreting the factors separately (e.g., different sources, age, burning conditions, wind direction etc.). In order to avoid any over interpretation of the PMF result only the recombined BBOA factor was discussed in the manuscript.

For PMF solutions with less than 6 factors no COA factor was separated and the biomass burning event was separated less clearly from factors not belonging to biomass burning. Therefore the 6-factor solution was chosen and split factors were recombined as described above.
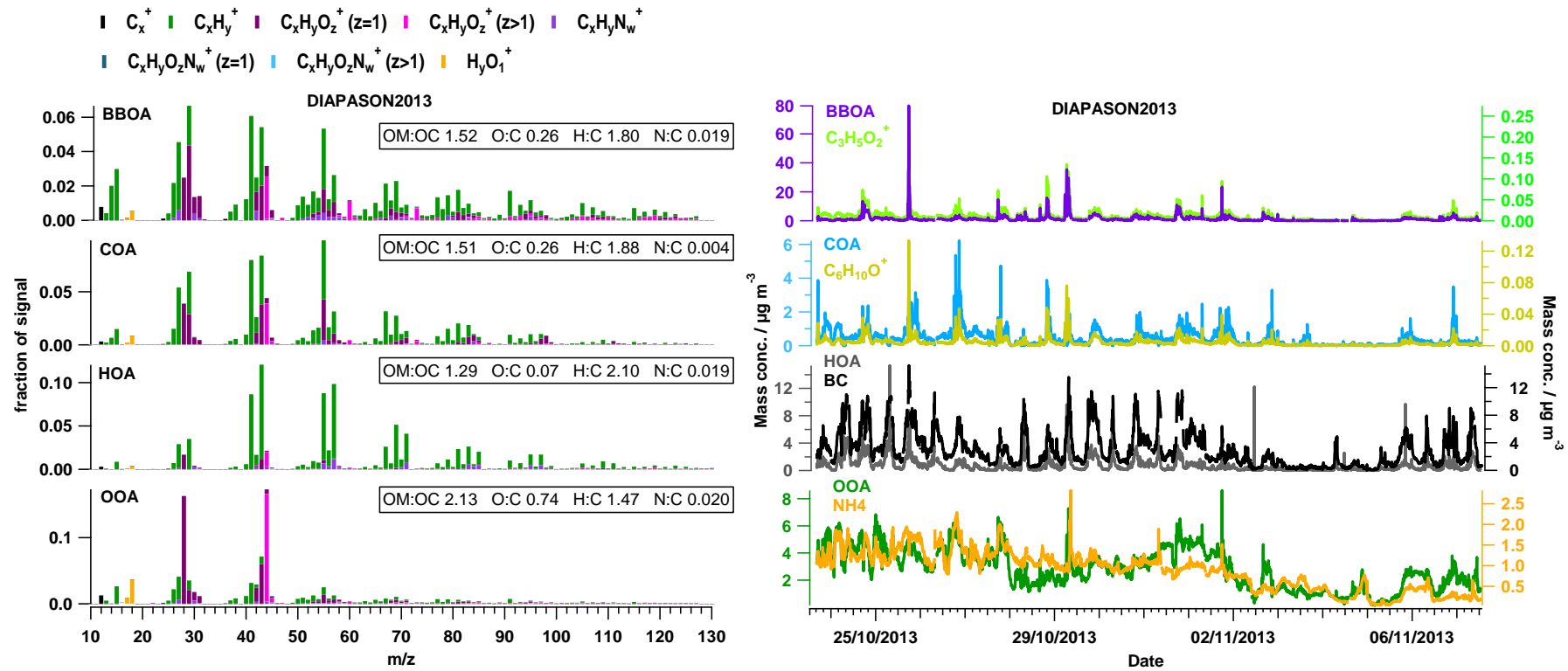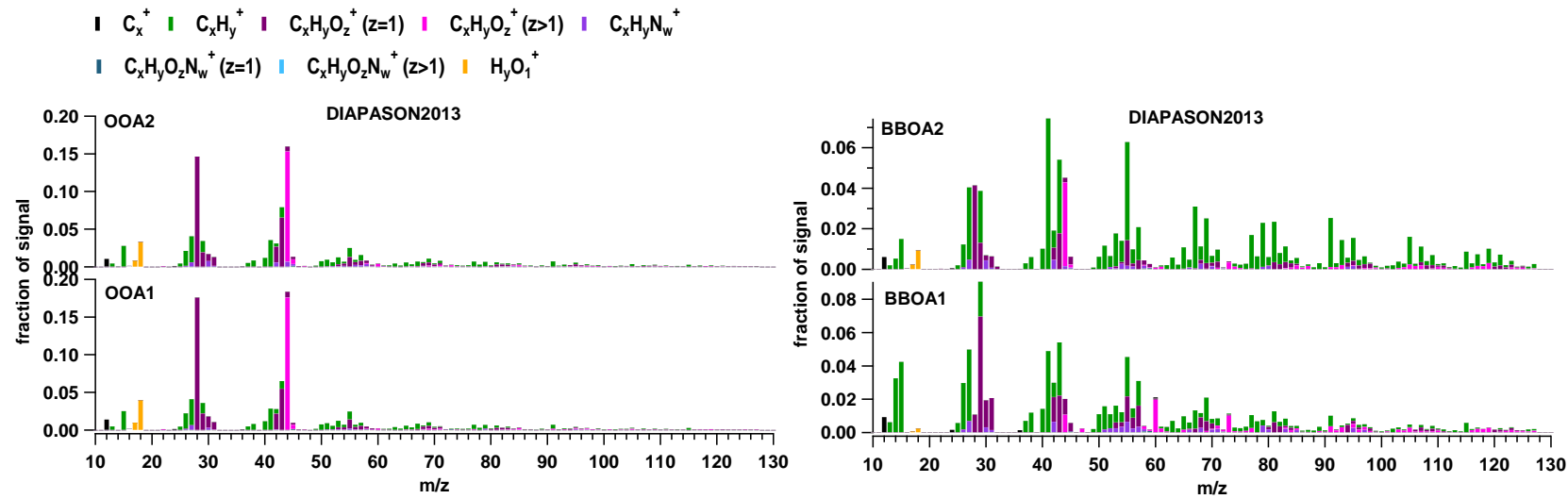
1

2   **Figure S5: HR mass spectra for OA factors (left) and time series of OA factors and ancillary data (right) for DIAPASON2013.**
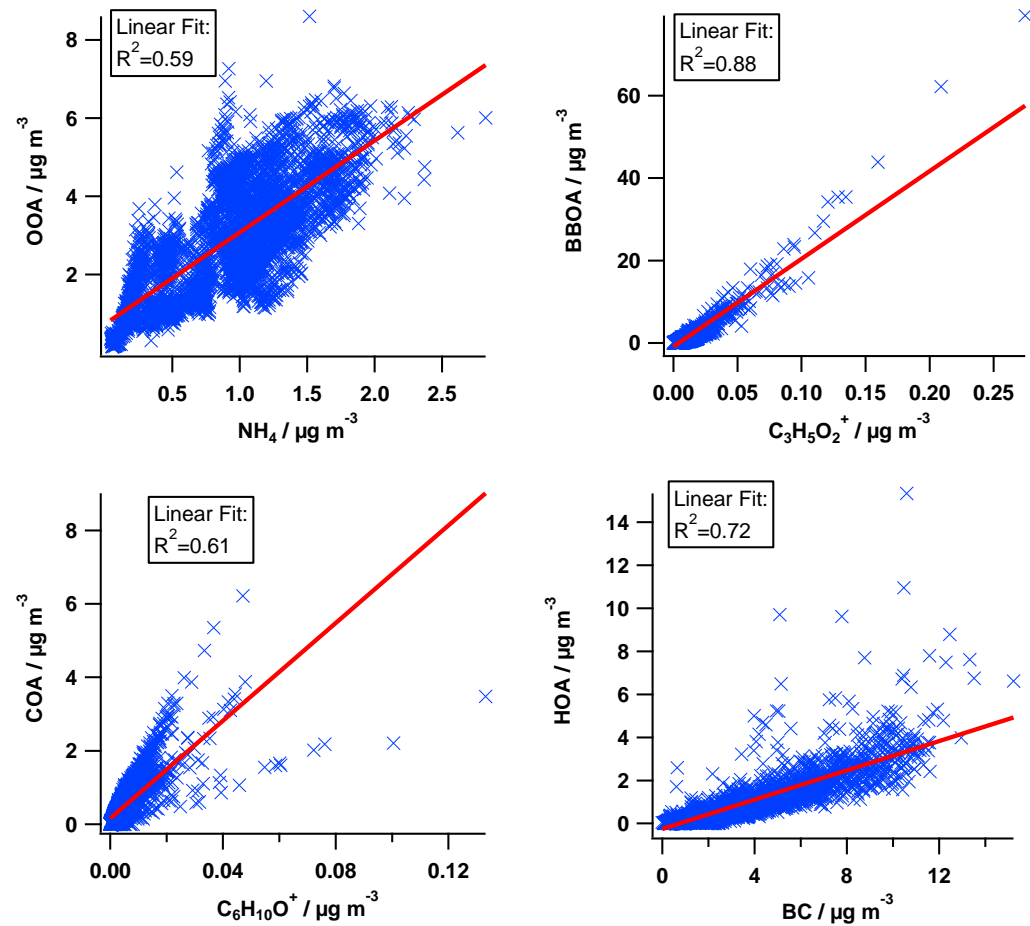
1

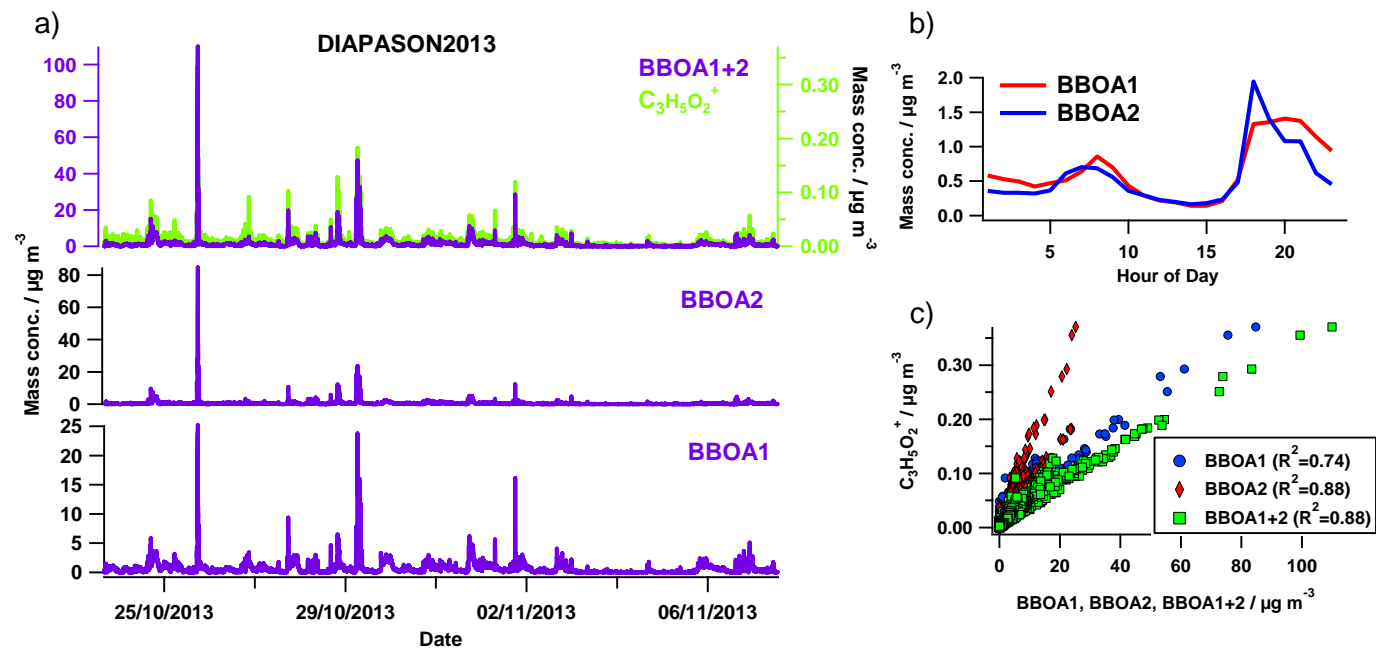2   **Figure S6: Scatter plots of PMF factors with external tracers for DIAPASON2013.**

3

Figure S7: Mass spectra of two factors assigned to OOA (left) and BBOA (right), which were recombined to one single OOA and BBOA factor, respectively.

Figure S8: a) Time series of BBOA1, BBOA2, the recombined factor BBOA1+2 and the biomass burning tracer $C_3H_5O_2^+$. b) Diurnal cycles of BBOA1 and BBOA2. c) Scatter plot of $C_3H_5O_2^+$ and the factors BBOA1, BBOA2 and BBOA1+2. Pearson's R^2 from linear regression of the data is shown for each factor.
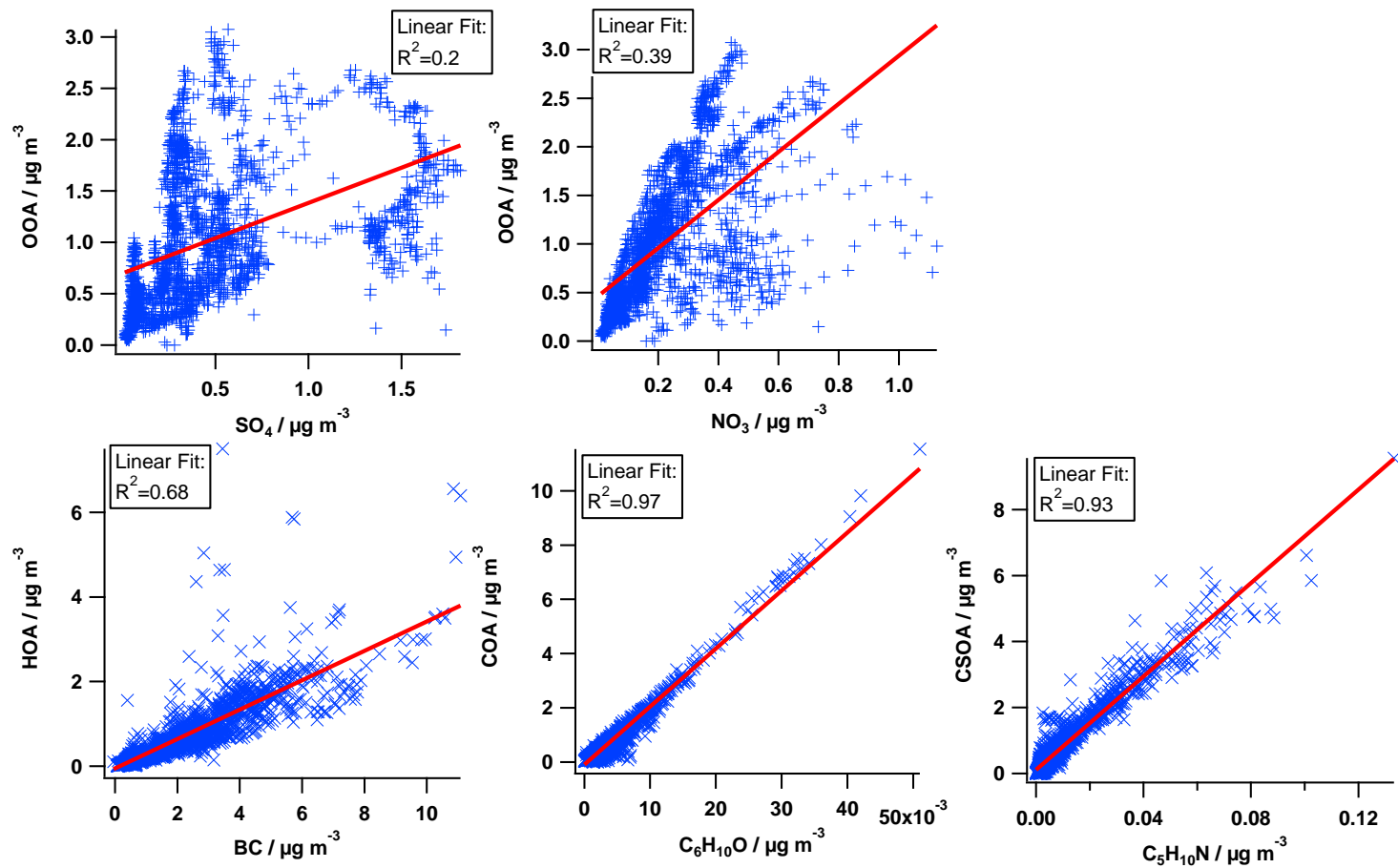
2.2   POPE2013

For POPE2013 a 4-factor solution was chosen (Figure S9). The 5-factor solution only produced a splitting of the OOA factor, whereas in the 3-factor solution the factors CSOA and HOA were not separated. Factors were identified based on their mass spectra and correlations with external tracers (Figures S9 and S10). The OOA factor shows only poor correlation with SO_4 but slightly better correlation with NO_3, suggesting a local contribution to this factor or significant advection of nitrate.
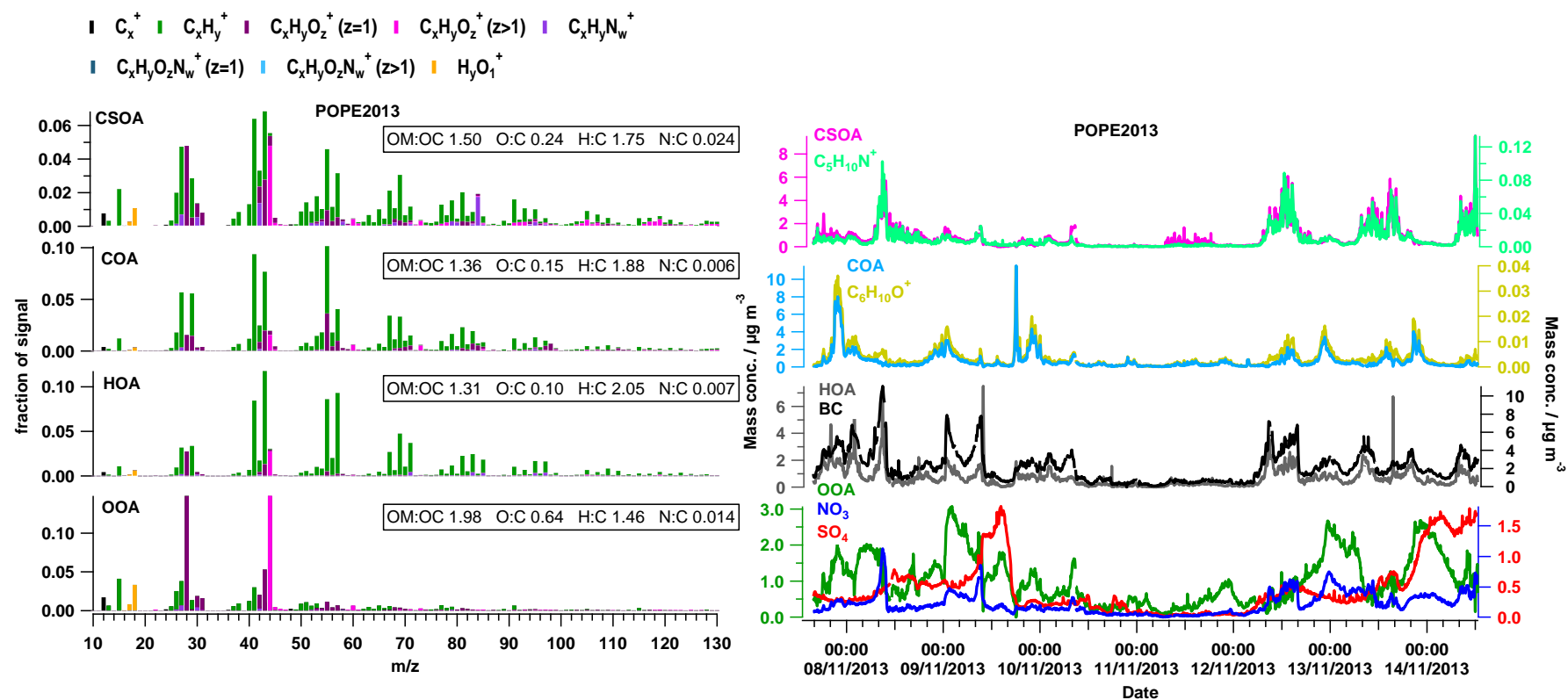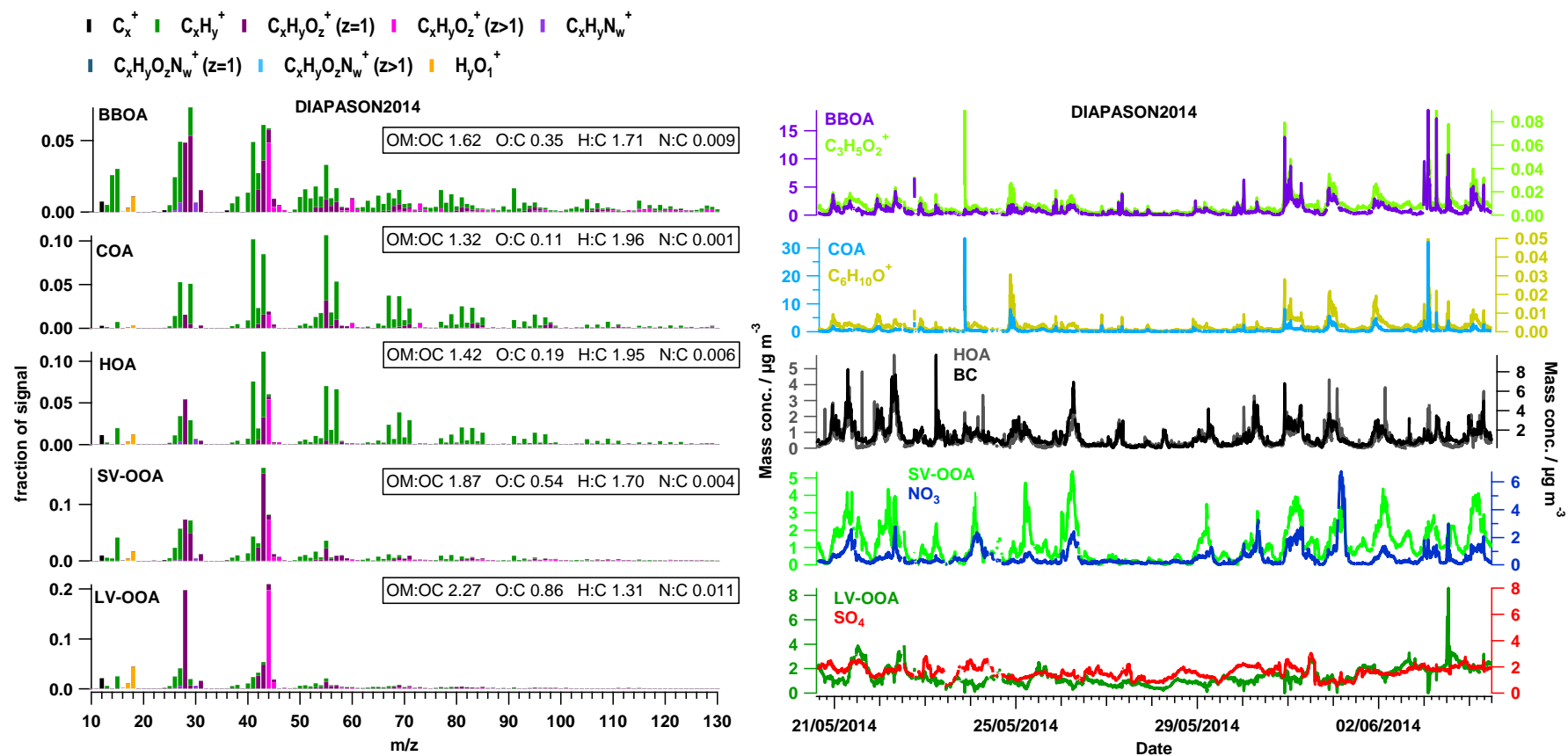

Figure S9: HR mass spectra for OA factors (left) and time series of OA factors and ancillary data (right) for POPE2013.
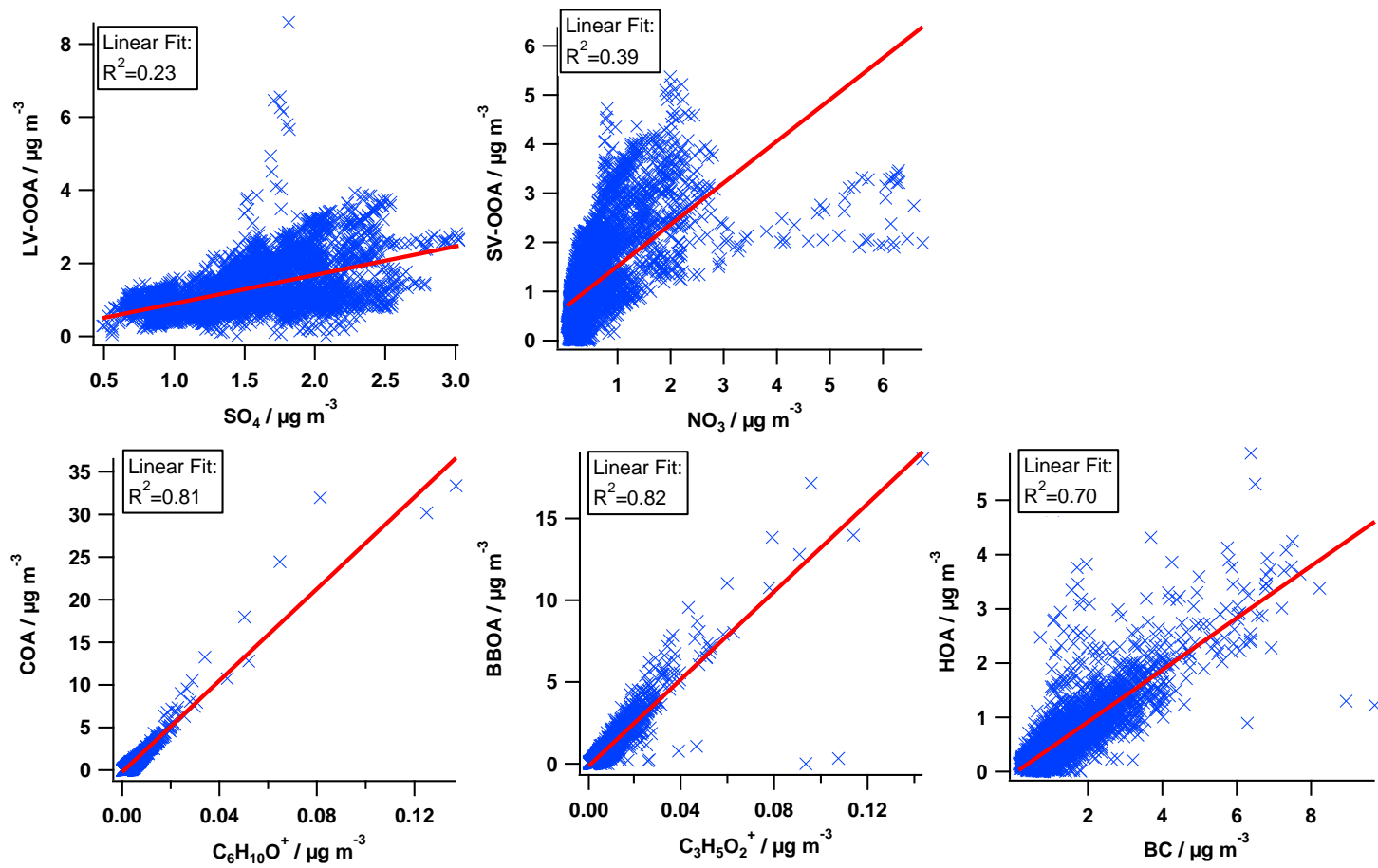
1

2 **Figure S10: Scatter plots of PMF factors with external tracers for POPE2013.**

3

1 **2.3 DIAPASON2014**

2 For DIAPASON2014 a 5-factor solution was chosen (Figure S11). In the 6-factor solution LV-OOA was split into two factors and in the 4-factor solution the

3 factors BBOA, HOA and COA were not fully separated, but distributed over two factors. Factors were identified based on their mass spectra and correlations

4 with external tracers (Figures S11 and S12).

6 **Figure S11: HR mass spectra for OA factors (left) and time series of OA factors and ancillary data (right) for DIAPASON2014.**

1

2   **Figure S12: Scatter plots of PMF factors with external tracers for DIAPASON2014.**

3

1 ## 2.4 POPE2014

2 For POPE2014 a 6-factor solution was chosen. In this solution two factors assigned to LV-OOA (LV-OOA1 and LV-OOA2) were recombined to one LV-OOA

3 (Figure S14), using the sum of the time series and the weighted average of the mass spectra. The spectra of LV-OOA1 and LV-OOA2 (Figure S13) showed a

4 correlation of R^2=0.96. In the 5-factor solution HOA was not separated, which is why the 6-factor solution was chosen instead. In Figure S14 the mass spectra

5 and time series for the OA types found for POPE2014 are shown; in Figure S15 correlations used to identify the aerosol types are presented.
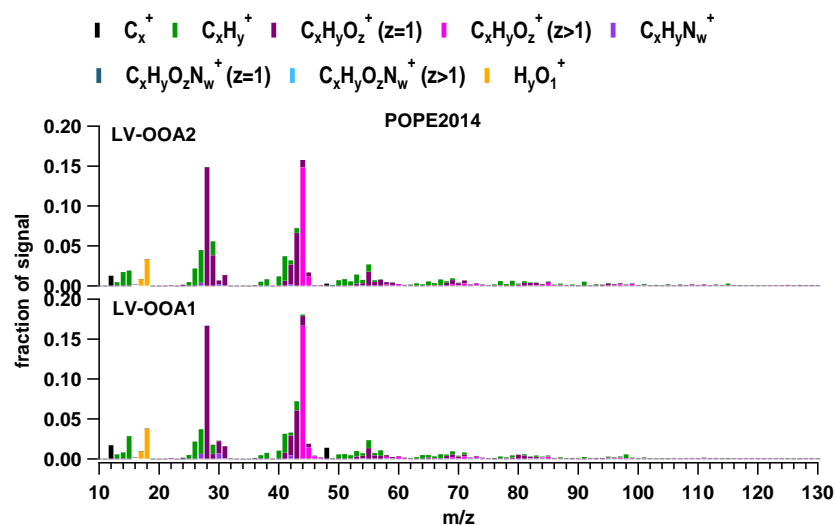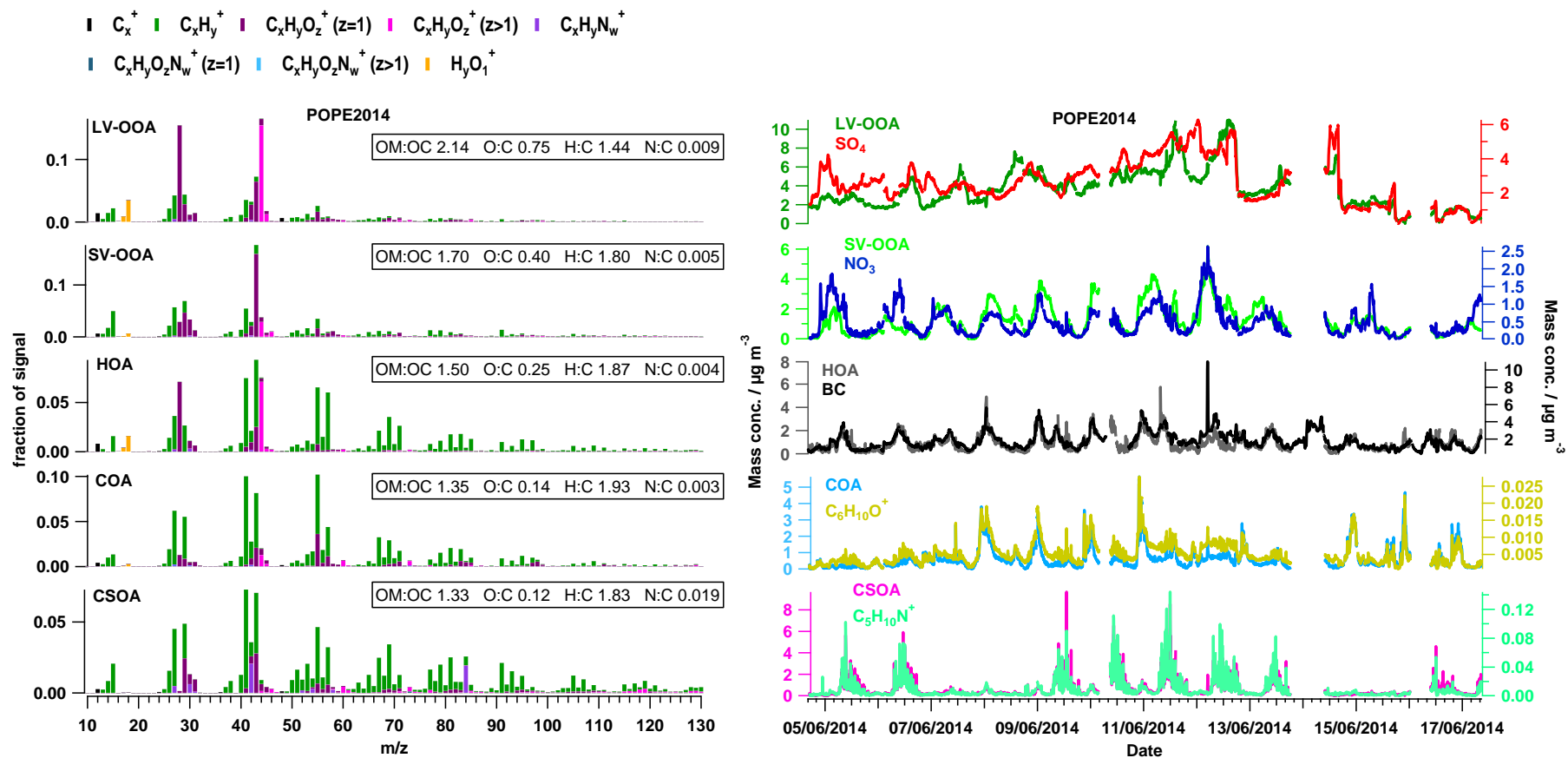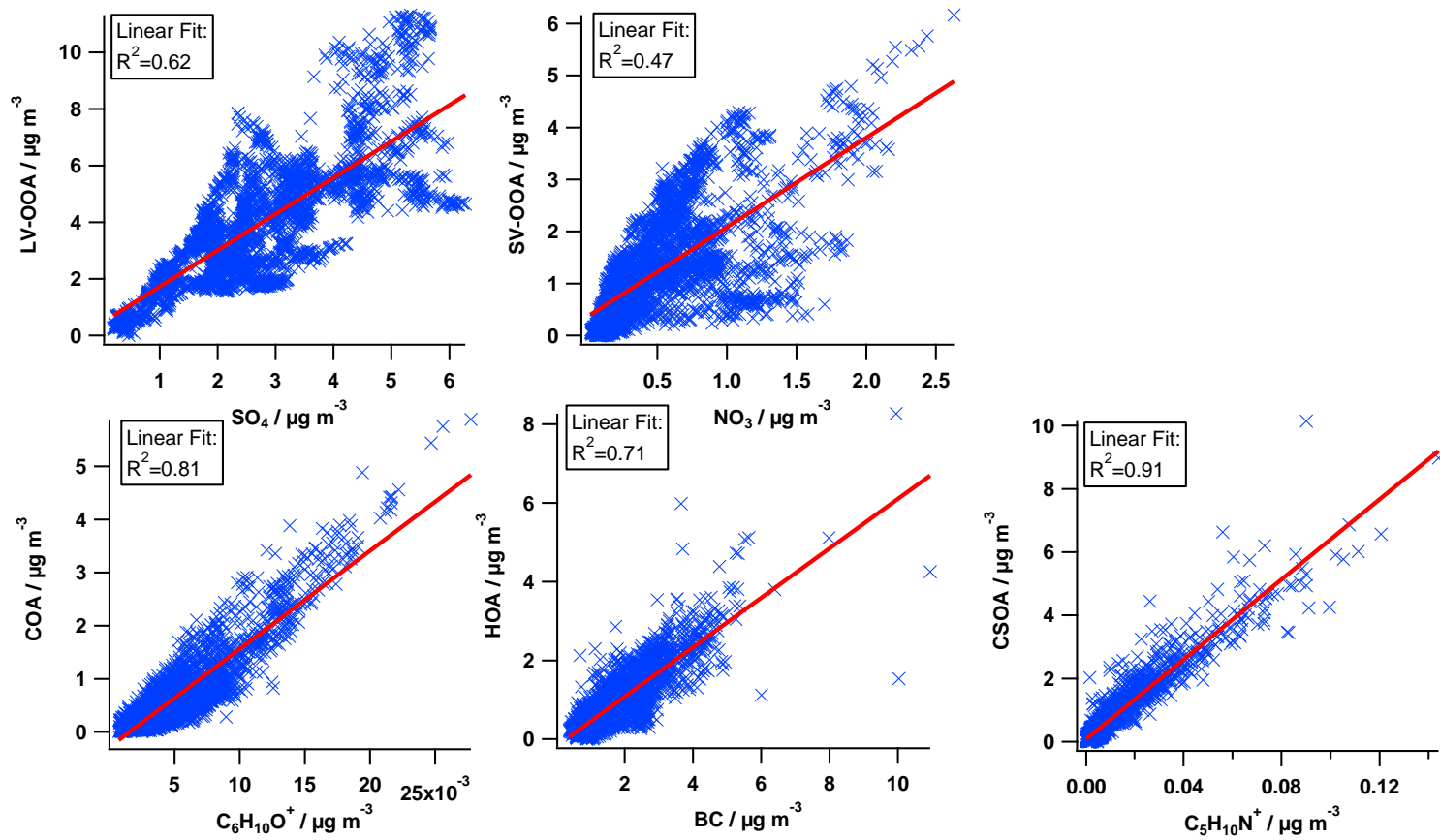
6

7

8 **Figure S13: Mass spectra of two factors assigned to LV-OOA, which were regrouped to one single LV-OOA factor.**

9

1

2

3 **Figure S14: HR mass spectra for OA factors (left) and time series of OA factors and ancillary data (right) for POPE2014.**

Figure S15: Scatter plots of PMF factors with external tracers for POPE2014.

1 **2.5 CSOA**

2 An AMS raw spectrum around m/z 84 of a 30s run during a period of increased CSOA concentration is presented in Figure S16. The contribution of the proposed

3 nicotine tracer fragment $C_5H_{10}N^+$ to the m/z 84 signal is clearly visible.
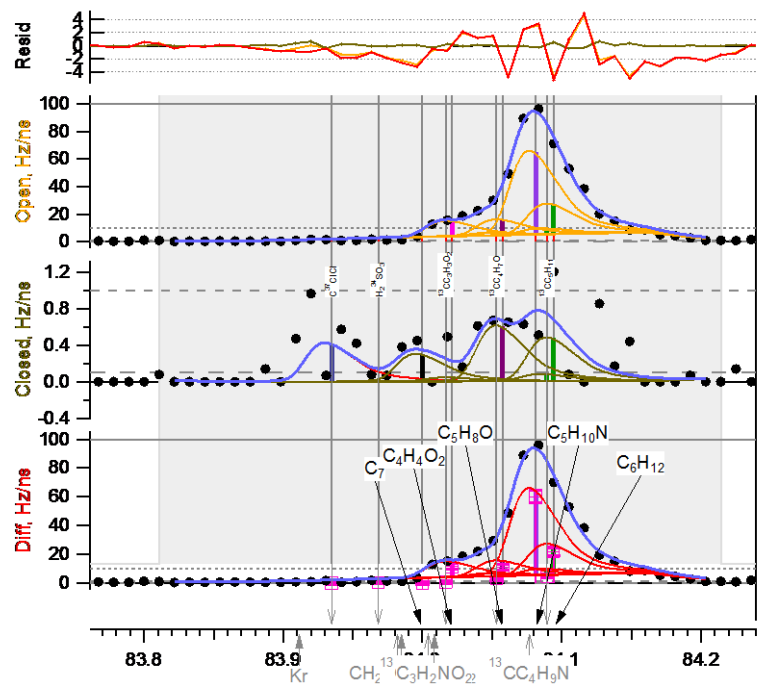
4

5 **Figure S16: m/z 84 of a raw spectrum for a 30 s run during a period of increased CSOA concentrations during POPE2014.**

6

7

1   **References**

2   Canagaratna, M. R., Jayne, J. T., Jimenez, J. L., Allan, J. D., Alfarra, M. R., Zhang, Q., Onasch, T. B., Drewnick, F., Coe, H., Middlebrook, A.,

3   Delia, A., Williams, L. R., Trimborn, A. M., Northway, M. J., DeCarlo, P. F., Kolb, C. E., Davidovits, P., and Worsnop, D. R.: Chemical and

4   microphysical characterization of ambient aerosols with the aerodyne aerosol mass spectrometer, Mass Spectrometry Reviews, 26, 185-222, 2007.

5   Canagaratna, M. R., Jimenez, J. L., Kroll, J. H., Chen, Q., Kessler, S. H., Massoli, P., Ruiz, L. H., Fortner, E., Williams, L. R., Wilson, K. R.,

6   Surratt, J. D., Donahue, N. M., Jayne, J. T., and Worsnop, D. R.: Elemental ratio measurements of organic compounds using aerosol mass

7   spectrometry: characterization, improved calibration, and implications, Atmos. Chem. Phys., 15, 253-272, 2015.

8   Middlebrook, A. M., Bahreini, R., Jimenez, J. L., and Canagaratna, M. R.: Evaluation of Composition-Dependent Collection Efficiencies for the

9   Aerodyne Aerosol Mass Spectrometer using Field Data, Aerosol Science and Technology, 46, 258-271, 2012.

10   Mohr, C., DeCarlo, P. F., Heringa, M. F., Chirico, R., Slowik, J. G., Richter, R., Reche, C., Alastuey, A., Querol, X., Seco, R., Penuelas, J.,

11   Jimenez, J. L., Crippa, M., Zimmermann, R., Baltensperger, U., and Prevot, A. S. H.: Identification and quantification of organic aerosol from

12   cooking and other sources in Barcelona using aerosol mass spectrometer data, Atmos. Chem. Phys., 12, 1649-1665, 2012.

13   Ulbrich, I. M., Canagaratna, M. R., Zhang, Q., Worsnop, D. R., and Jimenez, J. L.: Interpretation of organic components from Positive Matrix

14   Factorization of aerosol mass spectrometric data, Atmos. Chem. Phys., 9, 2891-2918, 2009.

15